Absence of nesting in the charge-density-wave system 1T-VS_2 as seen by photoelectron spectroscopy

M. Mulazzi,[1] A. Chainani,[1,2] N. Katayama,[3] R. Eguchi,[1,4] M. Matsunami,[1,4] H. Ohashi,[5] Y. Senba,[5] M. Nohara,[3] M. Uchida,[6] H. Takagi,[3,6,7] and S. Shin[1,4]

[1]*Excitation Order Research Team, RIKEN, SPring-8 Centre, Sayo-cho, Hyogo 679-5148, Japan*

[2]*Coherent X-ray Optics Laboratory, RIKEN, SPring-8 Centre, Sayo-cho 679-5148, Japan*

[3]*Department of Advanced Materials, University of Tokyo, Kashiwa 277-8561, Japan*

[4]*Institute of Solid State Physics, University of Tokyo, Kashiwa, Chiba 227-8587, Japan*

[5]*JASRI/SPring-8, Sayo-cho, Hyogo 679-5198, Japan*

[6]*Magnetic Materials Laboratory, RIKEN, Wako 351-0198, Japan*

[7]*Correlated Electron Research Center (CERC), AIST, Tsukuba 305-8562, Japan*

(Received 26 May 2010; revised manuscript received 15 July 2010; published 18 August 2010)

We report on the electronic structure and Fermi surfaces of the transition-metal dichalcogenide 1T-VS_2 in the low-temperature charge-density-wave (CDW) ordered phase. Using soft x-ray angle-resolved photoemission spectroscopy (ARPES), we investigate the in-plane and out-of-plane vanadium- and sulfur-derived band dispersions and identify k_z dispersions in this layered system. Core-level photoemission and x-ray absorption spectroscopy show that vanadium electrons are in the d^1 configuration while $2p$-$3d$ resonant ARPES shows only $3d$-derived dispersive bands near the Fermi level. Comparison of energy- and angle-dependent data with band-structure calculations reveals renormalization of the $3d$ bands, but no lower Hubbard band, a signature of the rather weak electron-electron correlations in VS_2. High-resolution temperature-dependent low-energy ARPES measurements show the opening of an energy gap at the Fermi level that is attributed to the condensation of the CDW phase. The results indicate a CDW transition in the absence of nesting for 1T-VS_2

DOI: 10.1103/PhysRevB.82.075130 PACS number(s): 71.20.−b, 71.18.+y, 79.60.−i

I. INTRODUCTION

Transition-metal dichalcogenides show rich physics because of the interplay between electronic and phononic degrees of freedom in reduced dimensions. When the temperature is lowered under a critical value, the competition between the electronic and lattice energy minimization leads to the stabilization of a charge-density wave (CDW), i.e., a long-range order in which the valence-electron charge density acquires an extra periodicity (which may or may not be commensurate to that of the underlying lattice) that is not present in the high-temperature phase. The mechanism proposed by Peierls[1] about 60 years ago, based on the instability of a one-dimensional free-electron gas, with respect to a small shift in the atomic positions, gives a qualitative explanation of the CDW transition. This was recently questioned[2] for transition-metal dichalcogenides as too simple to explain the whole phenomenology of this class of materials in which Fermi-surface nesting, evolution of the CDW state into superconductivity[3] or Mott transition[4] is observed and sometimes coexist.

Similar to several other transition-metal dichalcogenide CDW systems,[5] VS_2, crystallizes in the 1T layered structure with one hexagonal plane of vanadium atoms alternating with two sulfur atom planes along the c axis. NMR experiments showed a CDW transition[6] with $T_{CDW}=308$ K and lead to the conclusion that nearly half of the Fermi surface is gapped in the low-temperature phase. The lattice parameters of VS_2 in the normal state are $a=3.219$ Å and $c=5.745$ Å,[7] while a two-dimensional CDW transition leads to a new unit cell with $a^*=3\sqrt{3}a$ and $c^*=c$. For this work,[8] large (5 mm $\times$5 mm$\times$10 μm) high-quality single crystals were synthesized and momentum-sensitive probes could be used to investigate the crystal structure, the CDW transition and the electronic structure of VS_2, beyond local probes such as x-ray absorption spectroscopy.[9]

In particular, while resonant angle-resolved photoemission spectroscopy (ARPES) has been reported for LaSb,[10] La metal,[11] and a few f-electron systems,[12] we present resonant soft x-ray ARPES (SX-ARPES) showing clear band dispersions for a $3d$ electron system.

II. EXPERIMENTAL AND THEORETICAL DETAILS

The SX-ARPES measurements were carried out at the a branch of the BL17SU beamline at SPring-8,[13] a soft x-ray beamline that can provide soft x rays in the 300–2000 eV energy range and of tunable polarization (s, p, and right circular and left circular). The photoelectrons with wave vectors along the ΓM (or AL) direction were collected at the same time in the angular acceptance range of the Scienta 2002 analyzer. Sweeping the sample tilt angle (rotation about the in-plane axis coincident with the analyzer acceptance direction) allowed the measurement of the ΓK direction. During the experiments circular polarization was used to avoid the effect of selection rules arising with linear polarization. No change in the line shapes and no carbon signal was observed in the 48 h of continuous measurements. The energy resolution was 200 meV, while the angular resolution was 0.2°, equivalent to a 0.04 Å^{-1} momentum resolution at 540 eV kinetic energy at normal emission. The crystal growth and characterization are described in Ref. 8. The samples were aligned by the orientation of the crystal planes with an accuracy of ≈3° and cleaved in vacuum at a temperature of

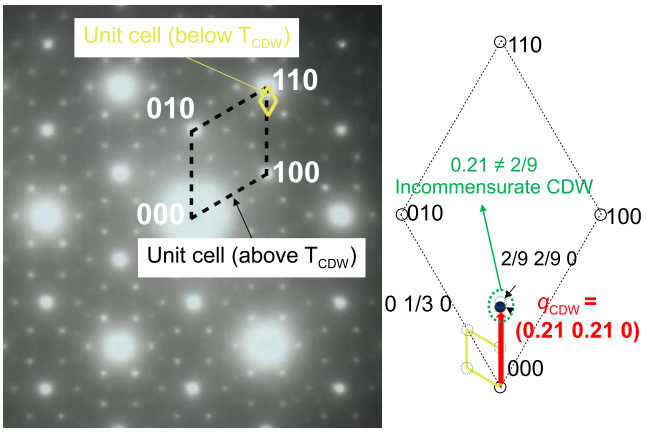

FIG. 1. (Color online) Left: electron-diffraction pattern obtained in a TEM of a VS_2 single crystal with the in-plane reciprocal space unit cell in the normal (black dashed lozenge) and CDW [yellow continuous small lozenge shifted on the (110) spot for clarity] phases. Right: schematic view of the reciprocal unit cells indicating that the experimental positions of the CDW-induced diffraction spots deviate from the commensurate superlattice case: the CDW vector is indicated by a fat red (or gray) arrow.

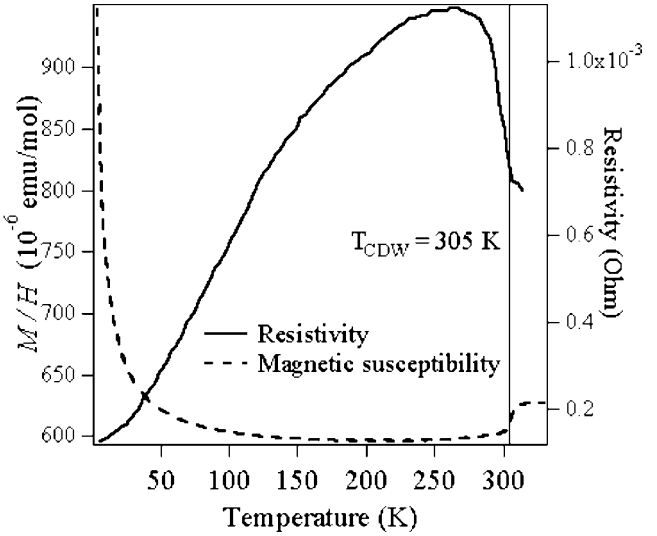

FIG. 2. Magnetic susceptibility (dashed line) and electrical resistivity (continuous line) of the VS_2 single crystal. The CDW transition is signaled by the jump in the magnetic susceptibility and the electrical resistivity at 305 K (marked by the vertical line).

20 K at a pressure better than 2×10^{-10} mbar. All SX-ARPES measurements were carried out at 20 K. The Debye temperature of VS_2 is not known, but assuming that it is similar to that of VSe_2 ($\Theta_D^{VSe_2}=220$ K), it is understood[14,15] that temperature-dependent soft x-ray ARPES measurements above the CDW temperature would yield indirect transition-dominated spectra.

The low-energy ARPES measurements were done on single crystals obtained from the same batch of those used for the SX-PES experiments and were also cleaved in vacuum. We used two photon sources for the experiments: a 7 eV laser (described in Ref. 16) and a He lamp, giving 21.22 eV photons. The energy resolution for the 7 eV laser was measured to be around 4 meV while it is about 10 meV for the experiments done with the He lamp.

The band structure of VS_2 was calculated using the "QUANTUM ESPRESSO"[17] package using scalar-relativistic ultrasoft pseudopotentials in the generalized-gradient approximation (GGA) of the exchange-correlation functional. The calculations that we present have been done with relaxed lattice parameters using a cutoff of 30 Ry for the plane-wave energy and 300 Ry for the electronic charge. The number of k points was 144 in the irreducible part of the Brillouin zone.

III. RESULTS

A. Characterization

In Fig. 1, a transmission electron microscopy (TEM) diffraction pattern of VS_2 at $T<T_{CDW}$ identifies the superlattice peaks. As indicated in the right panel of Fig. 1, the CDW transition in VS_2 is incommensurate to the normal phase lattice: the experimentally determined superstructure peaks are located at the $(2/9-\delta,2/9-\delta,0)$ with $\delta=0.12$ marking the difference from the commensurate case (for which $\delta=0$).

In Fig. 2, the magnetic susceptibility and the electrical resistivity measurements are shown. The CDW phase transition is signaled by a step in both the curves at $T=305$ K: the magnetic susceptibility decreases to a minimum, a signature of the gapping of the Fermi surface, and then increases because of the dominant (at low temperatures) paramagnetic contribution of vanadium atoms possibly intercalated between the sulfur planes. However, the electrical resistivity shows a quadratic behavior as a function of the temperature, suggesting the presence of a finite density of electronic states at the Fermi level in the CDW phase.

B. Absorption and resonant photoemission

In Fig. 3 we present the x-ray absorption spectroscopy (XAS) data on the vanadium L_3 and L_2 edges and the photoemission spectrum of $2p$ core levels. The XAS spectrum can be compared to the experimental data[18] and theoretical calculations[19] to infer that in 1T-VS_2 the vanadium atoms are in a d^1 configuration. In the XAS data of VS_2, there is a clear peak at an energy lower than the energy of the main peak that is due to atomic multiplets of the d^1 configuration.[19]

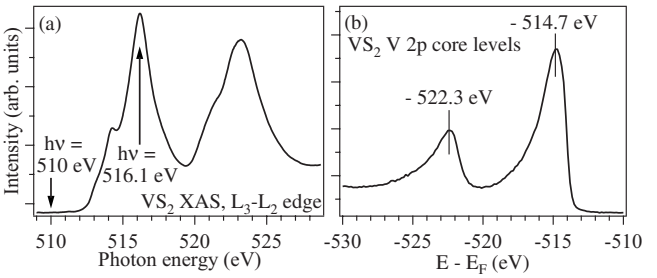

FIG. 3. (a) XAS of VS_2 single crystal across the L_3 and L_2 absorption edges and (b) angle-integrated photoemission spectrum of the vanadium $2p$ core levels. The ARPES data presented in the next figure have been obtained fixing the photon energy to the value for which the XAS spectrum is maximum ($h\nu=516.1$ eV).

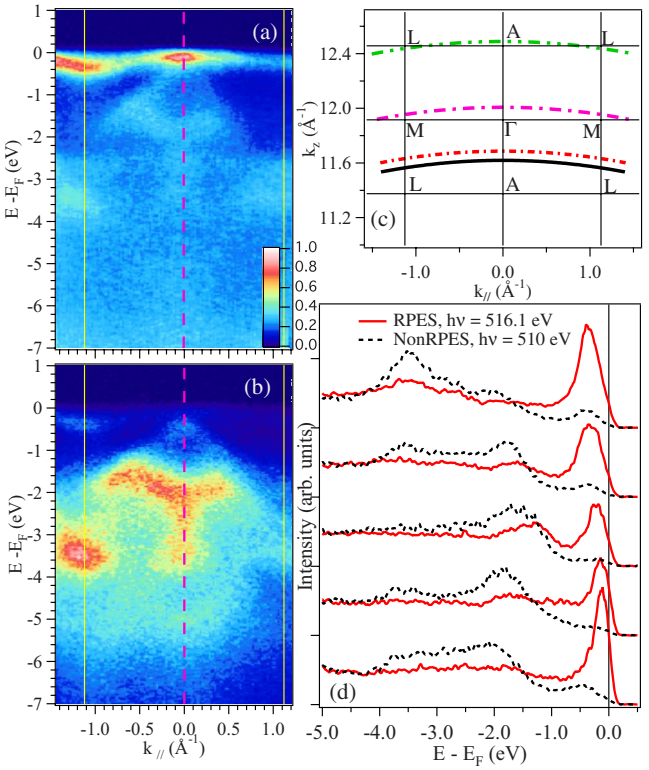

FIG. 4. (Color online) (a) RPES data taken with $h\nu$ =516.1 eV at the maximum of the vanadium L_3 absorption edge (as seen in Fig. 3); (b) Non-RPES data taken with $h\nu$=510 eV before the L_3 edge. The pink dashed and yellow continuous vertical lines in panels (a) and (b) mark the Brillouin-zone center and edge. (c) shows the reciprocal space in the repeated zone scheme together with the k points probed as a function of the kinetic energy and wave vector: $h\nu$=510 eV black line, $h\nu$=516.1 eV red large dashed-dotted line, $h\nu$=545 eV pink short dashed-dotted line, $h\nu$ =590 eV, green dashed-double-dotted line. (d) Line profiles taken from panels (a) and (b) at k points ranging from $k_{\|}$=0 Å^{-1} (bottom most) to $k_{\|}$=1.12 Å^{-1} (topmost) at steps of 0.28 Å^{-1}. At the bottom right of (a) the color scale (same also for the Figs. 5, 7, and 8) is indicated.

Similarly, the core-level photoemission spectra also indicate a binding energy typical of a d^1 configuration, i.e., V^{4+} (Ref. 20).

Figures 3(a) and 3(b) show SX-ARPES intensity maps obtained using $h\nu$=516.1 eV and $h\nu$=510 eV photons. These two photon energies correspond to the on- and off-resonant cases, obtained by tuning the photon energy near the L_3 absorption edge. The corresponding momenta probed in the Brillouin zone of VS_2 are shown in Fig. 3(c). Thus, using the $2p-3d$ resonance condition and comparing the on- and off-resonant data shown in Figs. 4(a) and 4(b), we could conclusively identify the vanadium d electrons as the main peak close to the Fermi level in the valence-band SX-ARPES data.

The vanadium d^1 electrons form bands at the Fermi level [the strong features in Fig. 4(a)] while the states at higher binding energies are derived from sulfur p electrons [stronger in Fig. 4(b)]. The vanadium d^1 electrons show an itinerant character with clear dispersions, as seen in Fig. 4(a) and

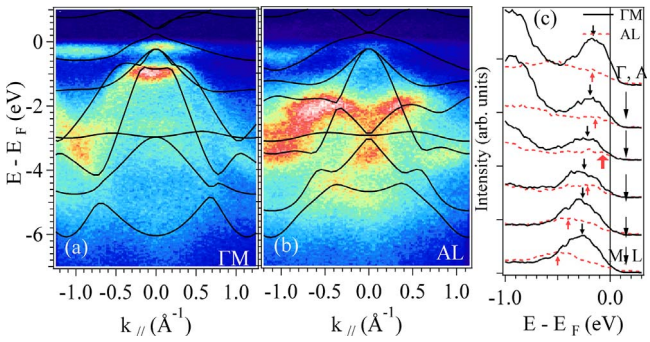

FIG. 5. (Color online) Band dispersion measured (a) along [with a 0.06 Å^{-1} k_z offset, as shown in Fig. 4(c)] the ΓM ($h\nu$ =545 eV) and (b) AL ($h\nu$=590 eV) directions. The black lines are the results of self-consistent band-structure calculations. (c) shows the bands near the Fermi level along ΓM (black continuous curves) and AL (red dashed curves): the former do not disperse while the latter do disperse and cross E_F. The approximate band position is indicated by black and red arrows for the two directions and k_F =−0.6 Å^{-1} is indicated by a thicker arrow.

in the energy distribution curves (EDCs) of Fig. 4(d). The comparison between the resonant and nonresonant data in Fig. 4(d) also reveals that the electron states within 1 eV from the Fermi level are hybridized bands made up of vanadium d states (nearest to E_F) and sulfur p states, with only the former showing a resonant behavior.

C. Soft x-ray valence-band ARPES

In Figs. 5(b) and 5(c) we show the band dispersion measured along two high-symmetry directions and compared to the calculations done at the experimentally probed k points. The calculated bands are in good qualitative agreement with the experimental ones. As seen in Fig. 5 the theoretical and the experimental band dispersion along ΓM differs from the one along AL. Since the two high-symmetry direction only differ in k_z, they should be equal in the case of an ideally two-dimensional electronic structure. For VS_2, since the GGA calculations reproduce the three dimensionality of the system, the k_z dependence cannot have a many-body origin. The vanadium d^1 electrons occupy the d_{z^2} orbitals,[5] which are oriented toward the sulfur atoms. This coupling to the sulfur and the rather small interlayer distance are the reasons for the three dimensionality of the system.

A similar result was previously found for the similar compound VSe_2,[21] for which the Fermi-surface crossing changes as a function of k_z. The band-structure calculations that we are presenting[17] here are in better agreement with the experiment than the ones calculated in Ref. 22. Specifically, the latter (i) predict the bottom of the valence band to lie at ≈−7.5 eV instead of about ≈−6 eV in the experiment, (ii) overestimate the energy distance between the sulfur and the vanadium bands, and (iii) give a bandwidth for the vanadium d bands of 0.7 eV instead of the experimental 0.5 eV. There is a discrepancy between theory and experiment: though the calculations indicate Fermi-level crossings along the ΓM and AL directions, the photoemission maps of Fig. 4, Fig. 5(a), and the EDCs of Fig. 5(c) (black curves) show that there is

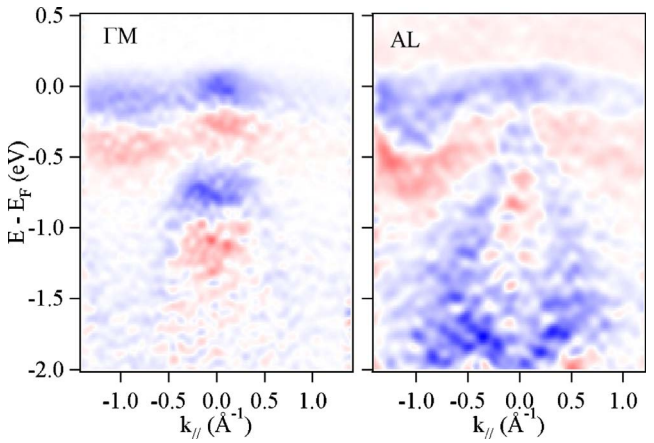

FIG. 6. (Color online) First derivative image, $\frac{dI(\vec{k},E)}{dE}$ of the data of Fig. 5 near the Fermi level plotted in false color ranging from blue (large negative) to red (large positive). The white lines separating the red/blue features indicate the binding energies of the vanadium bands as functions of the wave vector. The blue/red feature is not caused by the derivative of the Fermi-Dirac step normally arising in the energy derivative of the photoemission data. As it is easy to see, the blue/red feature is at least 0.3 eV away from the Fermi level. Thus it is genuinely derived from band dispersion of the vandium 3*d* states.

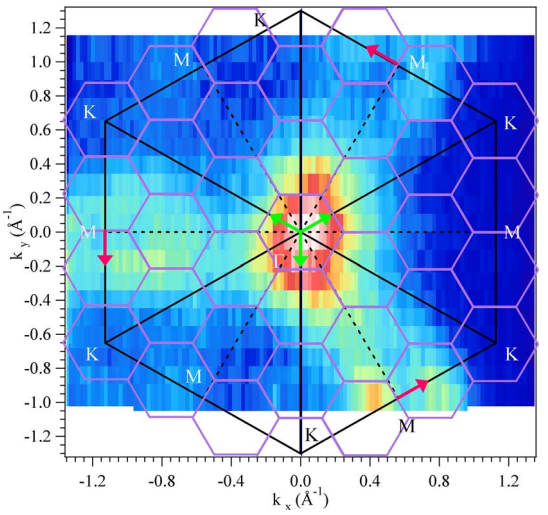

FIG. 7. (Color online) Unsymmetrized Fermi-surface mapping of VS_2 measured with $h\nu$=545 eV (k_z indicated in Fig. 4) and right circular polarization (integrating over a 160 meV energy window about E_F), probing the ΓMK plane of the Brillouin zone of the normal (black lines) or CDW (purple lines) phase. The green and pink arrows represent the experimental CDW vector at the Γ point or translated to the normal-state Brillouin-zone edge.

no Fermi-level crossing along ΓM in the CDW ordered phase. On the other hand, in the map in Fig. 5(b) and in the EDCs of Fig. 5(c) the band (red dashed curves) disperses and cross E_F at $k_{\|}$=−0.6 Å^{-1}. The same conclusion is obtained from the first derivative plot Fig. 6: the vanadium band never crosses the Fermi level along ΓM and it is flatter than the dispersion along AL.

We attribute the lack of Fermi crossings along ΓM to a band narrowing caused by electron-electron interactions for two reasons: (1) the V 3*d* bandwidth is about 0.5 eV in experiment while the calculations indicate a width of 0.7 eV. (2) Resonant ARPES data show that near the Fermi level there is finite intensity for all the *k* vectors probed. This is a signature that while a theoretical band is predicted to cross the Fermi level, in the experiment it is actually flatter and remains below E_F along ΓM. However, the observation of the *d* band dispersion effectively limits the strength of the electron-electron correlations. If they were too strong, a nondispersing lower Hubbard band indicative of Mott-Hubbard correlations should have been detected in photoemission. The vanadium *d* band bottom and group velocity at the M point [Fig. 5(a)] differ from those at the L point [Fig. 5(b)]. However, fitting both the experimental and theoretical bands with a simple parabola about the respective band bottoms, we infer that the experimental effective mass are about 20% heavier than the theoretical ones, both at the M and L points. Thus, the renormalization is effectively *k* independent.

In Fig. 7(a) we show the in-plane Fermi surface of VS_2 measured at a photon energy of 545 eV, probing the Brillouin zone in the ΓMK plane of the Brillouin zone. The experiment shows a strongly threefold, not sixfold, symmetric intensity distribution. A similar, though weaker, threefold symmetry has been found in 1T-VSe_2.[23] The threefold symmetry is not caused by the gapping of the Fermi surface: if we assume a BCS-type CDW gap, a signature of the opening of a CDW gap of $2\Delta_{CDW}=3.5k_BT_{CDW}\sim 92$ meV (the expected width at zero temperature), should be measurable even with a 200 meV energy resolution. However, in the data of Figs. 7(a) and 7(b), no gap or band folding is observed but the photoemission intensity is depressed at some wave vectors. Thus, the Fermi-surface symmetry follows from the threefold crystal lattice symmetry about the *c* axis.

D. Low-energy ARPES

The data presented in Fig. 8 are measured about the Γ point at two different temperatures for the two excitation sources employed. The intensity maps in the left panel [Figs. 7(a) and 7(b)] were taken at temperatures lower than T_{CDW} (8.2 K for the He lamp data and 100 K for the laser data) and the intensity maps in the central panel were taken at T =330 K$>T_{CDW}$. In the right panel, we compare the EDCs measured at the Γ point for the two temperatures, in order to check for spectral changes across T_{CDW}=305 K.

The ARPES maps of Figs. 8(b) and 8(d) show a hole band dispersion, positioned at about −0.5 eV of binding energy (at the Γ point) and a flat nondispersive band near the Fermi level (though less visible in the high-temperature data but clearly seen in the EDCs). This flat bands lies within 100 meV from the Fermi level, i.e., an energy range on the order of the Debye energy. In the comparison between the EDCs, it is possible to see that, upon decreasing the temperature below the T_{CDW}, mainly two things happen: (1) there is a clear depression of the intensity at the Fermi level; (2) the peak lying within 200 meV from the Fermi level becomes stronger with a temperature decrease. Because of k_z dispersion, the strong peak that is observed in the laser-PES data disappears from the binding energy range shown. As a side effect, the

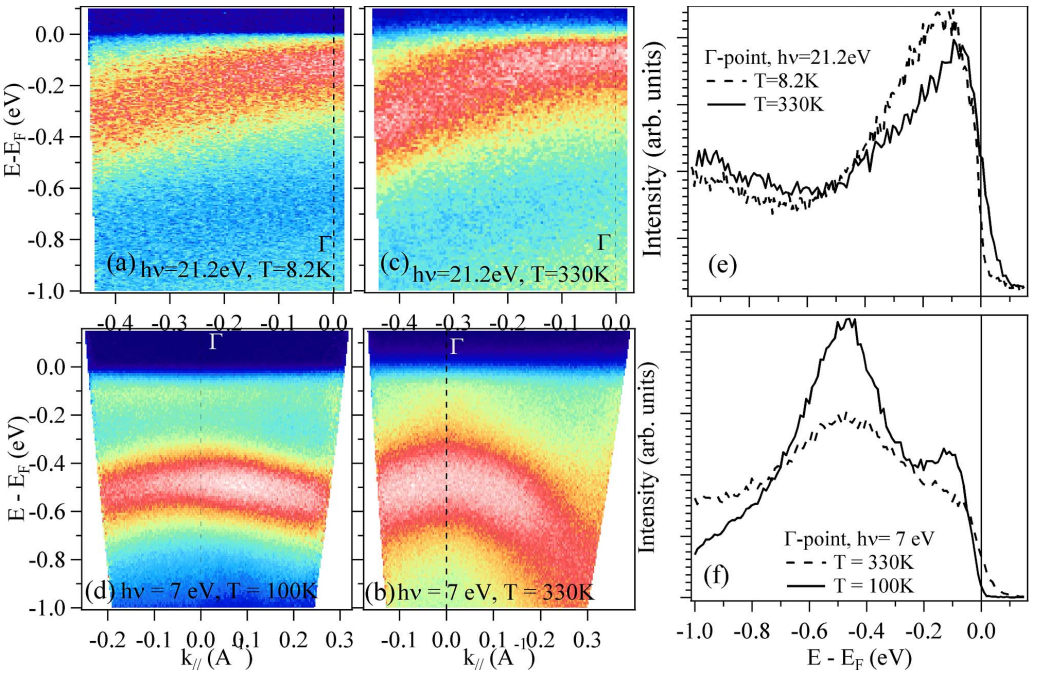

FIG. 8. (Color online) Angle-resolved photoemission maps taken with [(a) and (c)] helium lamp and [(b) and (d)] a laser source, for temperatures below and above the CDW transition temperature (T_{CDW}=305 K). In panels (e) and (f), a comparison of the EDCs extracted from the respective ARPES maps at the Γ point are plotted to show the temperature-dependent spectral changes across the phase transition.

spectra at high temperature are broader than those at lower temperature. We conclude that the above-described observations are the signature of the formation of a gap near the Fermi level. However, this gapping of the Fermi surface does not occur at the $\vec{q}_{CDW}$ determined by the TEM diffraction experimental data shown in the Fig. 1. On the contrary, the gapping occurs at least also at q=0 Å^{-1}, a value that does not allow for nesting of the Fermi surface. Because of the wave vector limitations caused by the photoelectrons low kinetic energies, it was not possible to explore the reciprocal space near Brillouin-zone edges, where the data of Fig. 7 show the Fermi-surface crossings.

IV. DISCUSSION

A. Fermi-surface nesting

The high transition temperature, the degree of three dimensionality of the electronic structure of 1T-VS_2, and the $\vec{q}_{CDW}$ determined by the TEM experiments do not support a Fermi-surface nesting picture, as was discussed earlier for TiS_2.[5] In fact, as seen in Fig. 7 the CDW vector (along any of the three equivalent ΓK lines) cannot join the straight sections of the Fermi surface because their magnitude is about half of what is necessary for a nesting scenario. These observations are consistent with the picture that the CDW transition does not necessarily occur at the experimental $\vec{q}_{CDW}$ and that the Fermi-surface nesting is not driving the CDW phase transition.[2]

B. Electron-phonon coupling

The lack of evidence of Fermi-surface nesting in VS_2 calls for another mechanism responsible of the CDW ordering. As discussed in Ref. 2, the electron-phonon coupling might be responsible for the CDW formation and thus it would be interesting to relate the electronic structure to the phonon properties of VS_2. While no phonon properties of VS_2 have been reported in the literature, it is possible to infer the electron-phonon coupling constant λ if we assume the validity of the BCS mean-field theory,[24] as was done for VSe_2.[25] Using the formula that relates the d band binding energy ϵ_0=0.273 eV (at the M point) to the CDW transition temperature T_{CDW}=305 K and λ, $k_B T_{CDW}=1.14\epsilon_0 e^{-1/\lambda}$, we obtain λ=0.42, which is larger than that for VSe_2, consistent with the higher transition temperature of VS_2. However, we note two important aspects of our data: (1) given the momentum dependence of ϵ_0 we obtain a 20% variation in λ over the Brillouin-zone points probed, a variation that is caused by the momentum dependence of the electronic structure, not of the phonon properties of VS_2; (2) only the vanadium electrons, in the d^1 configuration, form the Fermi surface of VS_2, while the sulfur bands lie at higher binding energies. This implies that the CDW formation primarily involves the coupling between the vanadium d electrons and the phonons.

Although, this analysis is not completely rigorous, it indicates that the application of the BCS formula is problematic to the present case because: (1) the experimental data show a clear absence of nesting while the BCS theory assumes perfect nesting; (2) in the BCS theory, the electron-phonon coupling is isotropic while the inferred k dependence of ϵ_0 implies a k-dependent electron-phonon coupling. These results, taken together with the fact that a naive estimate of λ for VS_2 is higher than that of VSe_2, hint at the role of an anisotropic electron-phonon coupling in VS_2. Further theoretical studies, based on an anisotropic electron-phonon coupling in VS_2 and

in the absence of nesting, are required to resolve the origin of the CDW transition in VS_2.

C. Conclusions

We measured the electronic structure of the layered dichalcogenide VS_2 using ARPES excited with soft x rays and vacuum ultraviolet photons, core-level photoemission, and XAS. The vanadium electrons are in a d^1 configuration forming dispersive bands near the Fermi level. Comparison of the experimental data to density-functional band-structure calculations finding good agreement: both theory and experiment show three dimensionality in the electronic structure arising from the rather short interlayer distance and occupation of the vanadium d_{z^2} orbitals. We could show that a mild isotropic electron-electron interaction renormalizes the band velocity of the vanadium electrons by 20% of the bare electron mass. The band narrowing induced by the correlations results in suppressing a band crossing predicted by *ab initio* calculations. We could make a simple estimate of the electron-phonon coupling constant λ which affects the vanadium electrons near E_F. The results reinforce the view[2] that for VS_2, the Fermi-surface nesting is not the origin of the CDW transition.

ACKNOWLEDGMENTS

The Foreign Postdoctoral Researchers Program of RIKEN supported this work and the synchrotron-radiation experiments were performed at the BL17SU at SPring-8 with the approval of RIKEN (Proposal No. 20090033).

[1] R. E. Peierls, *Quantum Theory of Solids* (Oxford University Press, London, 1956).
[2] M. D. Johannes and I. I. Mazin, Phys. Rev. B **77**, 165135 (2008).
[3] T. Kiss, T. Yokoya, A. Chainani, S. Shin, T. Hanaguri, M. Nohara, and H. Takagi, Nat. Phys. **3**, 720 (2007).
[4] L. Perfetti, A. Georges, S. Florens, S. Biermann, S. Mitrovic, H. Berger, Y. Tomm, H. Höchst, and M. Grioni, Phys. Rev. Lett. **90**, 166401 (2003).
[5] P. Aebi, Th. Pillo, H. Berger, and F. Lévy, J. Electron Spectrosc. Relat. Phenom. **117-118**, 433 (2001); Z. Y. Wu, G. Ouvrard, P. Moreau, and C. R. Natoli, Phys. Rev. B **55**, 9508 (1997).
[6] T. Tsuda, H. Yasuoka, Y. Kitaoka, and F. J. Di Salvo, J. Magn. Magn. Mater. **31-34**, 1101 (1983).
[7] D. W. Murphy, C. Cros, F. J. Di Salvo, and J. V. Waszczk, Inorg. Chem. **16**, 3027 (1977).
[8] N. Katayama, Ph.D. thesis, Tokyo University, 2008.
[9] Y. Ohno, H. Watanabe, A. Kawata, S. Nakai, and C. Sugiura, Phys. Rev. B **25**, 815 (1982).
[10] C. G. Olson, P. J. Benning, M. Schmidt, D. W. Lynch, P. Canfield, and D. M. Wieliczka, Phys. Rev. Lett. **76**, 4265 (1996).
[11] S. L. Molodtsov, M. Richter, S. Danzenbächer, S. Wieling, L. Steinbeck, and C. Laubschat, Phys. Rev. Lett. **78**, 142 (1997).
[12] T. Okane, T. Ohkochi, Y. Takeda, S.-i. Fujimori, A. Yasui, Y. Saitoh, H. Yamagami, A. Fujimori, Y. Matsumoto, M. Sugi, N. Kimura, T. Komatsubara, and H. Aoki, Phys. Rev. Lett. **102**, 216401 (2009).
[13] H. Ohashi, Y. Senba, H. Kishimoto, T. Miura, E. Ishiguro, T. Takeuchi, M. Oura, K. Shirasawa, T. Tanaka, M. Takeuchi, K. Takeshita, S. Goto, S. Takahashi, H. Aoyagi, M. Sano, Y. Furukawa, T. Ohata, T. Matsushita, Y. Ishizawa, S. Taniguchi, Y. Asano, Y. Harada, T. Tokushima, K. Horiba, H. Kitamura, T. Ishikawa, and S. Shin, *Synchrotron Radiation Instrumentation: Ninth International Conference on Synchrotron Radiation Instrumentation*, AIP Conf. Proc. No. 879 (AIP, New York, 2007), p. 523.
[14] F. Venturini, J. Minár, J. Braun, H. Ebert, and N. B. Brookes, Phys. Rev. B **77**, 045126 (2008).
[15] L. Plucinski, J. Minár, B. C. Sell, J. Braun, H. Ebert, C. M. Schneider, and C. S. Fadley, Phys. Rev. B **78**, 035108 (2008).
[16] T. Kiss, F. Kanetaka, T. Yokoya, T. Shimojima, K. Kanai, S. Shin, Y. Onuki, T. Togashi, C. Zhang, C. T. Chen, and S. Watanabe, Phys. Rev. Lett. **94**, 057001 (2005).
[17] P. Giannozzi, S. Baroni, N. Bonini, M. Calandra, R. Car, C. Cavazzoni, D. Ceresoli, G. L. Chiarotti, M. Cococcioni, I. Dabo, A. Dal Corso, S. de Gironcoli, S. Fabris, G. Fratesi, R. Gebauer, U. Gerstmann, C. Gougoussis, A. Kokalj, M. Lazzeri, L. Martin-Samos, N. Marzari, F. Mauri, R. Mazzarello, S. Paolini, A. Pasquarello, L. Paulatto, C. Sbraccia, S. Scandolo, G. Sclauzero, A. P. Seitsonen, A. Smogunov, P. Umari, and R. M. Wentzcovitch, J. Phys.: Condens. Matter **21**, 395502 (2009).
[18] M. G. Brik, K. Ogasawara, H. Ikeno, and I. Tanaka, Eur. Phys. J. B **51**, 345 (2006); M. W. Haverkort, Z. Hu, A. Tanaka, W. Reichelt, S. V. Streltsov, M. A. Korotin, V. I. Anisimov, H. H. Hsieh, H.-J. Lin, C. T. Chen, D. I. Khomskii, and L. H. Tjeng, Phys. Rev. Lett. **95**, 196404 (2005).
[19] G. van der Laan and I. W. Kirkman, J. Phys.: Condens. Matter **4**, 4189 (1992).
[20] R. Eguchi, M. Taguchi, M. Matsunami, K. Horiba, K. Yamamoto, Y. Ishida, A. Chainani, Y. Takata, M. Yabashi, D. Miwa, Y. Nishino, K. Tamasaku, T. Ishikawa, Y. Senba, H. Ohashi, Y. Muraoka, Z. Hiroi, and S. Shin, Phys. Rev. B **78**, 075115 (2008).
[21] T. Sato, K. Terashima, S. Souma, H. Matsui, T. Takahashi, H. Yang, S. Wang, H. Ding, N. Maeda, and K. Hayashi, J. Phys. Soc. Jpn. **73**, 3331 (2004).
[22] H. W. Myron, Physica B **99**, 243 (1980).
[23] K. Terashima, T. Sato, H. Komatsu, T. Takahashi, N. Maeda, and K. Hayashi, Phys. Rev. B **68**, 155108 (2003).
[24] G. Grüner, *Density Waves in Solids* (Perseus, Cambridge, MA, 1994).
[25] G. V. Kamarchuk, A. V. Khotkevich, V. M. Bagatsky, V. G. Ivanov, P. Molinié, A. Leblanc, and E. Faulques, Phys. Rev. B **63**, 073107 (2001).